Journal of Power Sources 272 (2014) 991–996

Contents lists available at ScienceDirect

Journal of Power Sources

journal homepage: www.elsevier.com/locate/jpowsour

Hierarchical vanadium pentoxide microflowers with excellent long-term cyclability at high rates for lithium ion batteries

Liang Chen [a], Xin Gu [a], Xiaolei Jiang [a], Nana Wang [a], Jie Yue [a], Huayun Xu [a], Jian Yang [a, *], Yitai Qian [a, b, **]

[a] Key Laboratory of Colloid and Interface Chemistry, Ministry of Education, and School of Chemistry and Chemical Engineering, Shandong University, Jinan 250100, Shandong, PR China
[b] Hefei National Laboratory for Physical Science at Microscale, Department of Chemistry, University of Science and Technology of China, Hefei 230026, PR China

HIGHLIGHTS

- V_2O_5 microflowers composed of thin nanosheets are prepared by a two-step process.
- V_2O_5 microflowers exhibit a capacity of 126 mAh g^{-1} at 200 mA g^{-1} over 150 cycles.
- The capacity could retain at 104 mAh g^{-1} after 1500 cycles at 1 A g^{-1}.
- The performance can be associated with their structure and capacitive contribution.

GRAPHICAL ABSTRACT

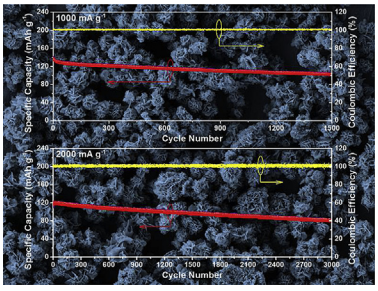

ARTICLE INFO

Article history:
Received 24 June 2014
Received in revised form
2 September 2014
Accepted 5 September 2014
Available online 16 September 2014

Keywords:
Vanadium oxide
Solvothermal synthesis
Hierarchical structure
Lithium ion batteries

ABSTRACT

Hierarchical V_2O_5 microflowers composed of thin nanosheets have been achieved by a solvothermal reaction first and then a low-temperature calcination. These micro-flowers are characterized by powder X-ray diffractometer (XRD), scanning electron microscope (SEM), and transmission electron microscope (TEM). The nanoscale size and sheet-like structure of the building blocks in V_2O_5 microflowers make them a promising cathode material for lithium ion batteries. After 1500 cycles at a current density of 1 A g^{-1}, the reversible capacity of V_2O_5 microflowers is kept at 104 mAh g^{-1}. Even at a rate of 2 A g^{-1}, the reversible capacity is still above 80 mAh g^{-1} after 3000 cycles. The excellent electrochemical properties of V_2O_5 microflowers are associated with their unique structure and capacitive feature.

1. Introduction

As a clean and reliable energy storage device, lithium-ion batteries (LIBs) have been widely applied in many portable electronics. But the electrode materials in the commercial LIBs could not meet the needs for large energy density and high power density. Among the promising materials, vanadium oxides constructed by layered structures are very attractive for LIBs. Due to a variety of oxidation states of vanadium (+5, +4, +3, and +2), there is a rich chemistry associated with them [1]. In various vanadium oxides, V_2O_5 has been demonstrated as one of the appealing candidates due to its low cost and high abundance as well as high theoretical capacity. However, V_2O_5 suffers from its low ionic diffusivity (10^{-12}–10^{-13} cm^2 s^{-1}) [2,3] and its bad structure stability, leading to low capability and poor cyclability.

* Corresponding author. Tel./fax: +86 531 88364489.
** Corresponding author. Key Laboratory of Colloid and Interface Chemistry, Ministry of Education School of Chemistry and Chemical Engineering, Shandong University, Jinan 250100, Shandong, PR China. Tel.: +86 531 88366360.
E-mail addresses: yangjian@sdu.edu.cn (J. Yang), ytqian@ustc.edu.cn (Y. Qian).

http://dx.doi.org/10.1016/j.jpowsour.2014.09.048
0378-7753/

In order to address these issues, many efforts have been devoted to the controls on the size, shape and structure of V_2O_5. As a result, various nanostructures of V_2O_5, such as nanoparticles [4–6], nanorods [7], nanotubes [8], nanowires [9,10], nanobelts [11,12] and nanosheets [13,14], have been synthesized and evaluated as electrode materials. Nanoscale size of these structures could increase the electroactive surface area, shorten the diffusion distance of Li^+, and alleviate the mechanical stress upon cycling, all of which promotes the rate capability and cycling stability. However, nanostructures always give rise to low volumetric energy density [15], which is against their applications in LIBs. Moreover, the expanded contact between electrolyte and nanostructures is also likely to enhance side reactions and reduce thermal stability [15]. In light of this, the assembly of nanostructures into hierarchical microparticles might be a good solution. Based on this concept, Lou et al. synthesized porous V_2O_5 micro-spheres composed of uniform nanofibers as a cathode for LIBs, which exhibited a specific capacity of 130 mAh g^{-1} after 100 cycles at 0.5C (~75 mA g^{-1}) [15]. Wang and Su fabricated porous V_2O_5 microspheres constructed of cross-linked nanobricks, which showed the reversible capacities of 100 and 85 mAh g^{-1} over 100 cycles at 0.5C and 1C (1C = 150 mA g^{-1}) [16]. Mai and his coworkers prepared porous V_2O_5 microplates by the thermolysis of NH_4VO_3 [17]. The microplates preserved the reversible capacities of 123 and 108 mAh g^{-1} after 100 cycles at 1 A g^{-1} and 2 A g^{-1}. The same group fabricated V_2O_5 microflowers by a supercritical solvothermal reaction followed by a high-temperature calcination [18]. These microflowers kept a discharge capacity of 108 mAh g^{-1} after 200 cycles at 10C (1C = 147 mAh g^{-1}). However, this preparation of V_2O_5 microflowers is time-consuming, which needs at least 9 days. Recently, hollow microflowers composed of V_2O_5 nanosheets were obtained by a similar but efficient procedure [19]. The hollow microflowers could deliver a discharge capacity of ~130 mAh g^{-1} after 100 cycles at 300 mAh g^{-1}. But the hollow structures reduce the volumetric energy density.

Herein, hierarchical V_2O_5 microflowers are synthesized by a time-efficient and facile process. These microflowers constructed by discrete and thin nanosheets, exhibit excellent electrochemical properties for lithium storage, particularly for the long-term cycling at high rates. They could preserve a reversible capacity of 104 mAh g^{-1} after 1500 cycles at a current density of 1000 mA g^{-1}. Even after 3000 cycles at 2000 mA g^{-1}, the specific capacity is still kept above 80 mAh g^{-1}. These V_2O_5 microflowers not only present the longest cycle life to the best of our knowledge, and also the ultralow fading rate per cycle. The outstanding performances are associated with their structure and the capacitive component in the specific capacity.

2. Experiment section

2.1. Materials synthesis

In a typical procedure, NH_4VO_3 (0.77 g) and oxalic acid (1.25 g) in a molar ratio of 2:3 were dissolved in 10 mL of deionized water, producing a dark green solution. Then, 2 mL of this solution was added into 35 mL of isopropanol. Due to the decreasing of the solvent polarity, some solutes precipitated from the solution. The suspension was centrifuged to obtain a clear solution. After that, the solution was transferred into a Teflon-lined stainless steel autoclave with a capacity of 45 mL and kept at 200 °C for 6 h. The resulting product was collected and washed with deionized water and absolute ethanol thoroughly. After dried at 60 °C overnight in a vacuum oven, the product was calcined at 350 °C for 2 h in air with a heating rate of 1 °C min^{-1} to produce highly-crystallized V_2O_5 microflowers.

2.2. Structure characterization

X-ray powder diffraction (XRD) patterns were achieved on a Bruker D8 advanced X-ray diffractometer with Cu Kα radiation (λ = 1.5418 Å). The structure and morphology of the products were observed by a field emission scanning electron microscope (SEM, SUPRA™ 55), a transmission electron microscope (TEM, JEM-1011) with an accelerating voltage of 100 kV. Nitrogen sorption isotherm was examined on a Micromeritics ASAP-2020HD88 instrument at 77 K.

2.3. Electrochemical measurements

The electrochemical tests were examined by CR2032 coin cells. The working electrode was composed of 70 wt% active material (V_2O_5), 20 wt% acetylene black as the conductive additive, and 10 wt% poly(vinylidene fluoride) (PVDF) as a binder. The slurry was coated on an aluminum foil and the coated foil was dried in vacuum at 60 °C. The resulting films were pressed and punched into the discs with a diameter of 12 mm and used as a cathode. The typical disk electrode contained active material of ~1 mg cm^{-2}. Then, it was assembled in an argon-filled glove box (Mikrouna, Super 1220/750/900) with a lithium foil as the counter and reference electrode, a mixture of 1 M $LiPF_6$ in ethylene carbonate (EC)–ethyl methyl carbonate (EMC)–dimethyl carbonate (DMC) (1:1:1 by volume) as the electrolyte, and a Celgard 2300 micro-porous membrane as the separator. Galvanostatic discharge–charge cycles of cells were performed at room temperature using Land CT2001A battery cycler (Xinnuo, Wuhan China) in a voltage range of 2.5–4.0 V at different current densities. Cyclic voltammetry (CV) was measured by a LK2005A electrochemical workstation between 2.5 V and 4.0 V at various scan rates. Electrochemical impedance spectra (EIS) were acquired on an Autolab Potentiostat Galvanostat (PGSTAT204) over a frequency range of 100 kHz to 0.01 Hz.

3. Results and discussion

The product obtained by a solvothermal reaction between ammonium vanadate and oxalic acid, is characterized with a field-emission scanning electron microscope (FESEM). As shown in Fig. S1A, the product consists of uniform flower-like micro-spheres with an average size of around 2 μm. The magnified FESEM image (Fig. S1B) reveals that the microflowers are assembled by many thin nanosheets, which is also confirmed by transmission electron microscope (TEM) images in Fig. S1C and D. The powder X-ray diffraction (XRD) pattern (Fig. S2) reveal the poor crystallinity of these microflowers and could not be attributed to any known vanadates.

After calcination at 350 °C for 2 h, these microflowers are converted to V_2O_5 with the same morphology. Fig. 1A shows the XRD pattern of these V_2O_5 microflowers (VFs). All the reflections can be indexed as orthorhombic-phase V_2O_5 (JCPDS card No. 41-1426, space group: *Pmmn*). It exhibits a unique layered structure in which the layers are constructed by square pyramids of [VO_5] *via* the edges and corners sharing (inset of Fig. 1A). This layered structure offers convenient pathways for lithium ions to diffuse in and out. The calculated lattice constants are 11.502 Å for *a*, 3.56 Å for *b*, 4.36 Å for *c*, very close to the reported ones (*a* = 11.51 Å, *b* = 3.565 Å, *c* = 4.372 Å). But the reflection intensity of {110} is extraordinarily high in comparison to the reported, suggesting the preferential growth of V_2O_5. This has been directly demonstrated by SEM and TEM images. As described in Fig. 1B, the product is predominant by a large number of rough microspheres with their sizes over 2–4 μm. A close-up view on the surface of a single microsphere (Fig. 1C and D) reveals that it is assembled by many

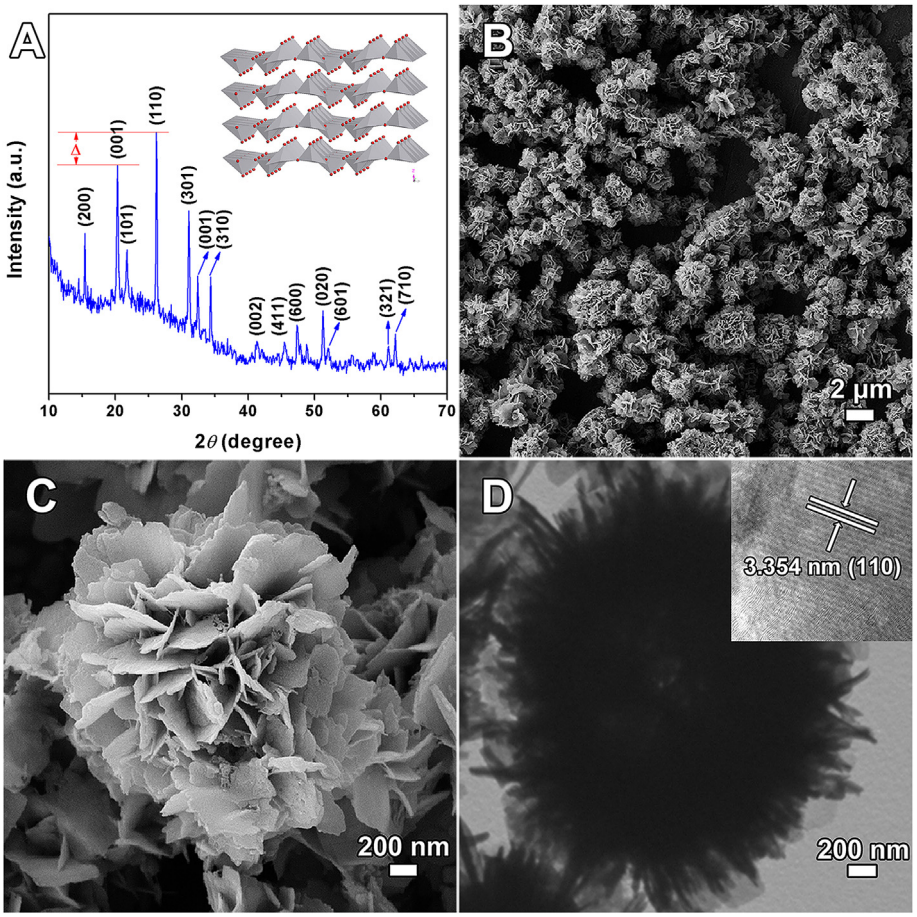

Fig. 1. (A) XRD pattern, (B and C) FESEM and (D) TEM images of V_2O_5 micro-flowers (VFs). The inset is a HRTEM image of V_2O_5 microflowers.

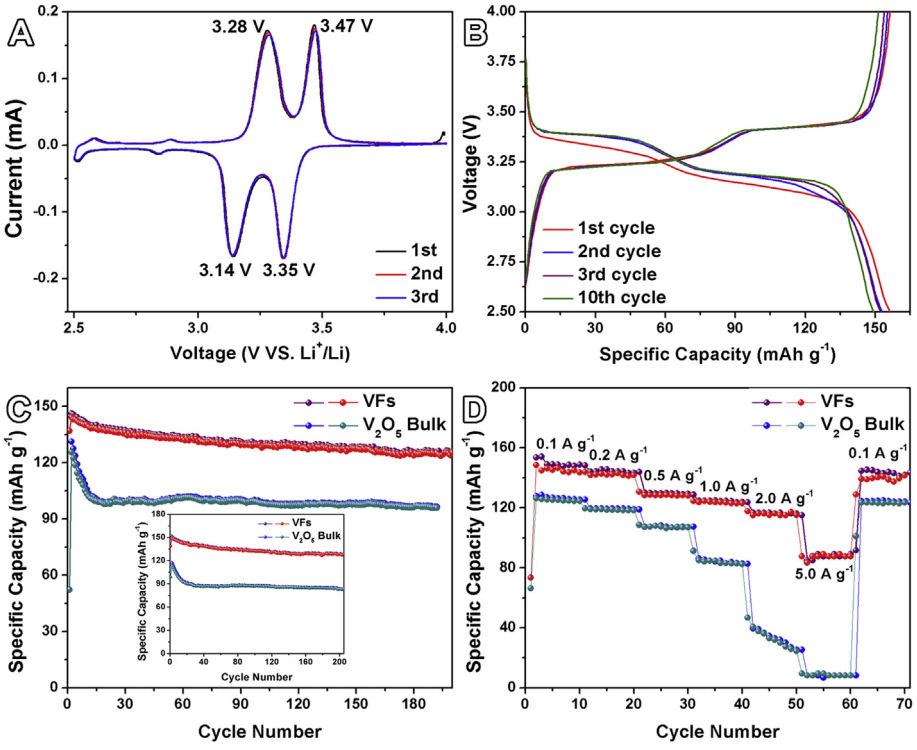

Fig. 2. (A) The first three consecutive cyclic voltammograms of the VFs at a scan rate of 0.1 mV s^{-1}; (B) discharge–charge voltage profiles of the 1st, 2nd, 3rd and 10th cycle at a current density of 100 mA g^{-1}; (C) cycling performances of VFs and bulk V_2O_5 at a current density of 200 mA g^{-1}. The inset is the cycling performances of VFs and bulk V_2O_5 at a current density of 500 mA g^{-1}; (D) rate performance of the VFs at various current densities.

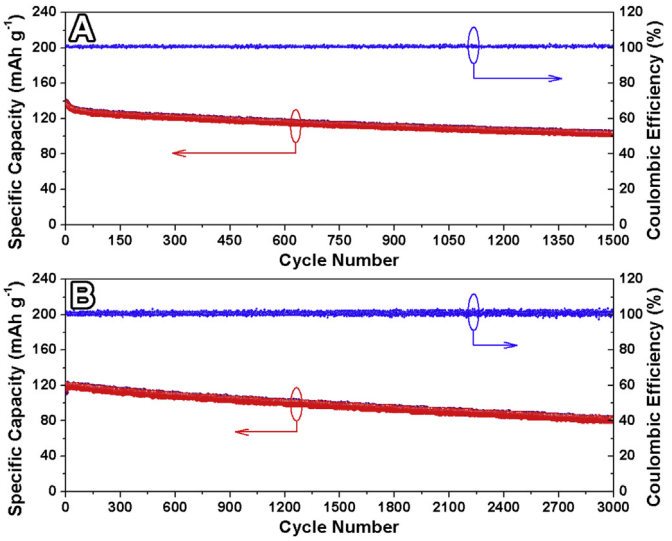

Fig. 3. (A) cycling performance and coulombic efficiency of the VFs at a current density of 1000 mA g^{-1}; (B) cycling performance and coulombic efficiency of the VFs at a current density of 2000 mA g^{-1}.

thin nanosheets with their average thickness of ~9 nm (Fig. S3), resulting in a flower-like structure. It is believed that the low calcination temperature and the slow heating rate enable this hierarchical structure survived from the calcination process. HRTEM image on the V_2O_5 microflowers (the inset of Fig. 1C) shows clear lattice fringes of {110} crystal planes of V_2O_5, consistent with the result from XRD pattern. In a viewpoint of lithium ion batteries, this hierarchical structure assembled by a large number of thin nanosheets, could increase the contact area between electrolyte and electrode, shorten the distance of lithium diffusion, as well as keep the electrode integrity, all of which are highly desirable for excellent lithium-storage performances [19,20]. The N_2 sorption isotherm of V_2O_5 microflowers is presented in Fig. S4. The isotherm exhibits a typical Type-II profile, giving a specific surface area of 15.9 m^2 g^{-1} based on Brunauer–Emmett–Teller (BET) theory.

The electrochemical properties of the VFs were evaluated by cyclic voltammetry (CV) at first. As shown in Fig. 2A, there are two intense peaks at 3.35 and 3.14 V vs. Li/Li^+ during the cathodic scan, which could be associated with lithium insertion from α-V_2O_5 to ε-$Li_{0.5}V_2O_5$ and then δ-LiV_2O_5 [21]. The anodic peaks at 3.28 and 3.47 V originate from the corresponding extraction of Li^+. It is noteworthy that the potential separations of the two redox pairs are only 0.14 and 0.12 V, both of which are significantly smaller than many reports [17–19]. For example, hollow V_2O_5 micro-flowers prepared by a solvothermal reaction at 200 °C for 12 h and then calcination at 350 °C for 2 h, exhibited the potential separations at 0.23 and 0.22 V [19]. Ultrathin V_2O_5 nanosheets achieved by a supercritical solvothermal reaction followed with a high-temperature annealing, presented the similar potential separations at 0.2 and 0.2 V for the redox pairs [18]. Very recently, porous V_2O_5 microplates obtained by the pyrolysis of NH_4VO_3, gave the potential separations at 0.15 and 0.22 V [17]. The small potential separation between the cathodic and anodic peaks, indicates the good reversibility of the insertion/extraction processes of lithium in V_2O_5. The CV profiles are kept as almost the same during the first three cycles, suggesting the high electrochemical stability. The excellent reversibility and stability make the electrode based on VFs appealing. The electrochemical performance of the VFs was evaluated by galvanostatic discharge–charge testing. Fig. 2B displays the discharge–charge curves of the VFs at a current density of 100 mA g^{-1}. They exhibit two plateaus at approximately 3.3 and 3.1 V vs. Li/Li^+, giving both discharge and charge capacities of 156 mAh g^{-1} for the first cycle. In the coming cycles, the discharge–charge curves does not change significantly, confirming the good reversibility of the insertion/extraction processes of Li^+ in VFs. This result is in good agreement with what observed from the CV profiles.

Fig. 2C illustrates the cycling performance of the electrode based on VFs over 2.5–4.0 V at a current density of 200 mA g^{-1}. Its specific capacity slowly decreases from 145 to 128 mAh g^{-1} after 150 cycles, corresponding to a very trivial fading rate of 0.08% per cycle. These capacities are apparently higher than those of bulk V_2O_5 (Fig. S5), which delivers 131 and 97 mAh g^{-1} for the 1st and the 150th cycle, respectively, resulting in a capacity decay rate of 0.17% per cycle. The capacity decay of the VFs electrode might be attributed to the formation of vanadium oxyfluorides induced by the $LiPF_6$ electrolyte upon cycling, which leads to mass loss of active materials [22,23]. As the current density increases to 500 mA g^{-1}, the cycle performance remains quite steady. On the contrary, the capacity of bulk V_2O_5 decreases rapidly, especially for the first few cycles as shown in the inset of Fig. 2C. To further evaluate the rate capability, the electrode of VFs was cycled at different current densities (Fig. 2D). At the current densities of 100, 200, 500, 1000, 2000, and 5000 mA g^{-1}, the specific capacities are 147, 144, 129, 125, 116, and 88 mAh g^{-1}. As the current density goes back to 100 mA g^{-1}, the specific capacity returns to 143 mAh g^{-1}, indicating the good stability of the electrode based on VFs. The rate performance of the VFs electrode is much better than those of bulk V_2O_5, particularly at high rates. At 5 A g^{-1}, the reversible capacity of bulk V_2O_5 decreases to only 10 mAh g^{-1}. The outstanding performance of VFs could be

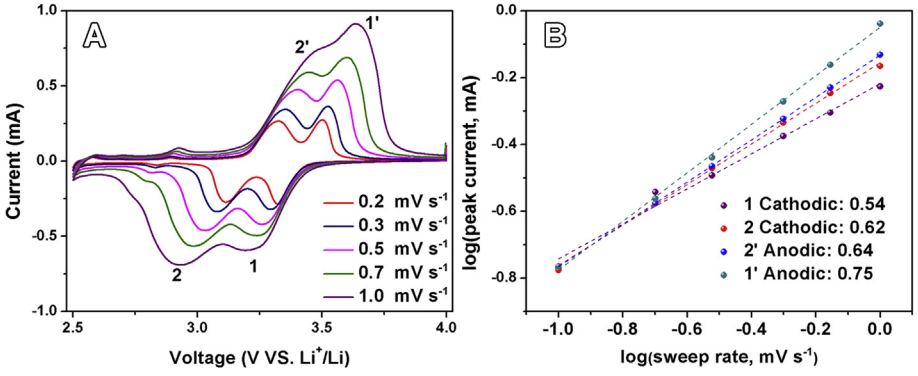

Fig. 4. (A) Cyclic voltammograms of the VFs at varying sweep rates; (B) log(peak current) *versus* log(sweep rate) of the VFs electrode.

assigned to its unique morphology. The flower-like structure composed by thin nanosheets, exhibits relatively large specific surface area and small subunit size, facilitating the quick diffusion of Li^+ and improving the rate performance. This could be verified by the estimation on the diffusion time of Li through the nanosheets, based on the equation of $t = L^2/D$. Here, t is the diffusion time of Li in the nanosheets, L is the thickness of the nanosheets ($L \approx 9$ nm), and D is the diffusion coefficient of Li for V_2O_5 ($D = 10^{-12}$ cm^2 s^{-1}) [24]. Thus, the diffusion time throughout the nanosheets is approximately 0.81 s, well supporting the outstanding high-rate capability. In addition, the thin nanosheets could efficiently relieve the mechanical stress generated by the insertion/extraction of Li during the discharge/charge processes [25,26].

The good cycling stability is further demonstrated by the long-term cycling at high rates, as shown in Fig. 3. At 1 A g^{-1}, the reversible capacity of VFs slowly drops from 138 to 104 mAh g^{-1} after 1500 cycles, which indicates a fading rate of 0.016% per cycle. Even at a rate of 2 A g^{-1}, the reversible capacity would be still kept above 80 mAh g^{-1} after 3000 cycles. The decaying rate turns into 0.010% per cycle. The fading rates are much smaller than the reported in literature [16–19,26]. Porous V_2O_5 microplates fabricated by the thermal decomposition of NH_4VO_3, gave the fading rates of about 0.054% per cycle after 100 cycles at 1 A g^{-1}, and 0.018% at 2 A g^{-1} [17]. The fading rate could be even higher for hollow V_2O_5 microflowers composed by many nanosheets, ~0.15% per cycle after 100 cycles at 300 mA g^{-1} [19]. For porous V_2O_5 microspheres obtained by the calcination of vanadyl glycolate, [16] the fading rate further increased to 0.25–0.28% per cycle. The small fading rate in our case confirms again the good cycling stability of VFs at high rates. Furthermore, this is the longest cycle life for V_2O_5-based electrodes to date, to the best of our knowledge.

The underlying insights for the excellent cyclability of VFs at high rates could be disclosed by CVs at different sweep rates. Fig. 4A shows the CVs of VFs at various sweep rates from 0.2 to 1.0 mV s^{-1}. As the sweep rate increases, the cathodic peaks shift to the negative voltage and the anodic peaks move to the positive, resulting in an enhanced electrode polarization. These peak currents (i_p) follow a power law relationship with the sweep rate (v), which could be described by the follow equation [27–29]:

$$i_p = av^b \quad (1)$$

where b as an important parameter could be achieved by the plot of log(peak current) *versus* log(sweep rate). If $b = 0.5$, the corresponding reaction is diffusion-controlled, which usually originates from the faradaic contribution due to lithium insertion or extraction. If $b = 1$, the reaction is surface-controlled, which could be associated with the faradaic contribution from pseudo-capacitor and/or the non-faradaic from double-layer capacitor. In our case, the b values are 0.64 and 0.75 for the anodic peaks, 0.54 and 0.62 for the cathodic peaks, as shown in Fig. 4B. The results indicate that there is a mixture of the above contributions for all these redox reactions. Moreover, the capacitive contribution is more significant for the anodic peak at 3.45 V, compared with the cases for the other peaks.

This significant feature of a capacitor behavior on VFs charged to 3.45 V is also confirmed by EIS spectra, as shown in Fig. 5. All the Nyquist plots at different voltages are composed by a depressed semicircle in the region of high-to-medium frequencies and a slope in the region of low frequencies. The depressed semicircle is related to the ohmic resistance (R_s) and the charge transfer resistance (R_{ct}). The slope is associated with the lithium diffusion inside electrode materials, which is usually evaluated by Warburg resistance (R_w) or a constant phase element (CPE). In the Nyquist plots of VFs discharged to 3.20 and 3.40 V, the phase angle of the slope is close to 45° (Fig. 5B), indicating a diffusion-controlled lithiation process basically. As the electrode is charged to 3.25 and 3.45 V, the phase angle of the slope greatly increases from 45° to 56.5°, as shown in Fig. 5C. This increasing of the phase angle suggests more capacitive contributions in the delithiation process at 3.45 V, which is consistent with the result from CVs.

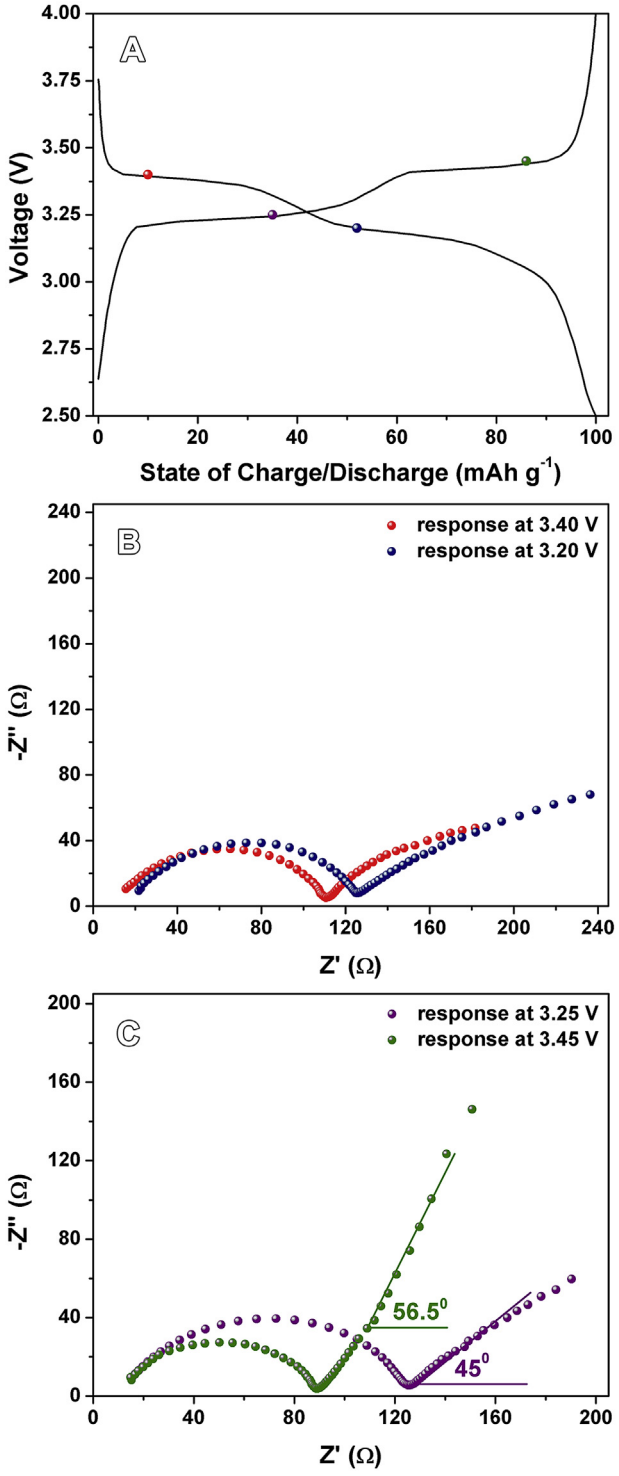

Fig. 5. (A) discharge–charge voltage profiles of VFs at the 4th cycle; (B, C) Nyquist plots of VFs discharged to 3.40 and 3.20 V (B) and charged to 3.25 and 3.45 V (C).

4. Conclusion

Hierarchical V_2O_5 microflowers are successfully synthesized by a solvothermal reaction followed by a calcination process at 350 °C. The microflowers with their sizes of 2–4 μm are composed by discrete and thin nanosheets with their thicknesses of 6–12 nm. The unique structure brings the great benefits for the cycling stability and rate capability of the microflowers, particularly for the long-term cycling at high rates. The hierarchical microflowers could keep a reversible capacity of 104 mAh g^{-1} after 1500 cycles at a rate of 1000 mA g^{-1}. Even over 3000 cycles at 2000 mA g^{-1}, the specific capacity is still above 80 mAh g^{-1}. The CVs profiles at different sweep rates reveal the considerable capacitive components in the specific capacity, which together with the unique morphology improves the cycling stability and rate capability.

Acknowledgment

This work was supported by the 973 Project of China (No. 2011CB935901), National Natural Science Foundation of China (Nos. 91022033, 51172076, 21203111, 21471090), New Century Excellent Talents in University (NCET-10-0369), Shandong Provincial Natural Science Foundation for Distinguished Young Scholar (JQ201205), Independent Innovation Foundations of Shandong University (2012ZD007), and New-faculty Start-up Funding in Shandong University.

Appendix A. Supplementary data

Supplementary data related to this article can be found at http://dx.doi.org/10.1016/j.jpowsour.2014.09.048.

References

[1] N.A. Chernova, M. Roppolo, A.C. Dillon, M.S. Whittingham, J. Mater. Chem. 19 (2009) 2526–2552.
[2] E. Potiron, A. Le Gal La Salle, A. Verbaere, Y. Piffard, D. Guyomard, Electrochim. Acta 45 (1999) 197–214.
[3] F. Lantelme, A. Mantoux, H. Groult, D. Lincot, J. Electrochem. Soc. 150 (2003) A1202–A1208.
[4] S.-H. Ng, T.J. Patey, R. Buchel, F. Krumeich, J.-Z. Wang, H.-K. Liu, S.E. Pratsinis, P. Novak, Phys. Chem. Chem. Phys. 11 (2009) 3748–3755.
[5] Y.N. Ko, J.H. Kim, S.H. Choi, Y.C. Kang, J. Power Sources 211 (2012) 84–91.
[6] C. Han, M. Yan, L. Mai, X. Tian, L. Xu, X. Xu, Q. An, Y. Zhao, X. Ma, J. Xie, Nano Energy 2 (2013) 916–922.
[7] H. Zhao, L. Pan, S. Xing, J. Luo, J. Xu, J. Power Sources 222 (2013) 21–31.
[8] X. Zhou, C. Cui, G. Wu, H. Yang, J. Wu, J. Wang, G. Gao, J. Power Sources 238 (2013) 95–102.
[9] L. Mai, L. Xu, C. Han, X. Xu, Y. Luo, S. Zhao, Y. Zhao, Nano Lett. 10 (2010) 4750–4755.
[10] E. Pomerantseva, K. Gerasopoulos, X. Chen, G. Rubloff, R. Ghodssi, J. Power Sources 206 (2012) 282–287.
[11] B. Li, Y. Xu, G. Rong, M. Jing, Y. Xie, Nanotechnology 17 (2006) 2560.
[12] Y. Wang, H.J. Zhang, K.W. Siah, C.C. Wong, J. Lin, A. Borgna, J. Mater. Chem. 21 (2011) 10336–10341.
[13] Z.L. Wang, D. Xu, L.M. Wang, X.B. Zhang, ChemPlusChem 77 (2012) 124–128.
[14] X. Rui, Z. Lu, H. Yu, D. Yang, H.H. Hng, T.M. Lim, Q. Yan, Nanoscale 5 (2013) 556–560.
[15] C. Zhang, Z. Chen, Z. Guo, X.W. Lou, Energy Environ. Sci. 6 (2013) 974–978.
[16] H.-E. Wang, D.-S. Chen, Y. Cai, R.-L. Zhang, J.-M. Xu, Z. Deng, X.-F. Zheng, Y. Li, I. Bello, B.-L. Su, J. Colloid Interface Sci. 418 (2014) 74–80.
[17] Q. An, P. Zhang, Q. Wei, L. He, F. Xiong, J. Sheng, Q. Wang, L. Mai, J. Mater. Chem. A 2 (2014) 3297–3302.
[18] Q. An, Q. Wei, L. Mai, J. Fei, X. Xu, Y. Zhao, M. Yan, P. Zhang, S. Huang, Phys. Chem. Chem. Phys. 15 (2013) 16828–16833.
[19] A.Q. Pan, H.B. Wu, L. Zhang, X.W. Lou, Energy Environ. Sci. 6 (2013) 1476–1479.
[20] L. Mai, Q. An, Q. Wei, J. Fei, P. Zhang, X. Xu, Y. Zhao, M. Yan, W. Wen, L. Xu, Small 10 (2014) 3032–3037.
[21] C. Delmas, H. Cognac-Auradou, J. Cocciantelli, M. Menetrier, J. Doumerc, Solid State Ionics 69 (1994) 257–264.
[22] Y.S. Cohen, D. Aurbach, Electrochem. Commun. 6 (2004) 536–542.
[23] J. Wu, N. Membreno, W.-Y. Yu, J.D. Wiggins-Camacho, D.W. Flaherty, C.B. Mullins, K.J. Stevenson, J. Phys. Chem. C 116 (2012) 21208–21215.
[24] J. Yan, A. Sumboja, E. Khoo, P.S. Lee, Adv. Mater. 23 (2011) 746–750.
[25] D. Rangappa, K. Sone, M. Wang, U.K. Gautam, D. Golberg, H. Itoh, M. Ichihara, I. Honma, Chem. Eur. J. 16 (2010) 6488–6494.
[26] D. Rangappa, K.D. Murukanahally, T. Tomai, A. Unemoto, I. Honma, Nano Lett. 12 (2012) 1146–1151.
[27] T. Brezesinski, J. Wang, S.H. Tolbert, B. Dunn, Nat. Mater. 9 (2010) 146–151.
[28] M. Sathiya, A. Prakash, K. Ramesha, J.M. Tarascon, A. Shukla, J. Am. Chem. Soc. 133 (2011) 16291–16299.
[29] V. Augustyn, J. Come, M.A. Lowe, J.W. Kim, P.-L. Taberna, S.H. Tolbert, H.D. Abruña, P. Simon, B. Dunn, Nat. Mater. 12 (2013) 518–522.